

Dynamic behaviours of black hole phase transitions near quadruple points

Jiayue Yang^{1,2}, and Robert B. Mann^{1,2}

¹*Department of Physics and Astronomy, University of Waterloo, Waterloo, Ontario, Canada, N2L 3G1*

²*Perimeter Institute, 31 Caroline Street North, Waterloo, ON, N2L 2Y5, Canada*

(Dated: September 21, 2023)

Treating the horizon radius as an order parameter in a thermal fluctuation, the free energy landscape model sheds light on the dynamic behaviour of black hole phase transitions. Here we carry out the first investigation of the dynamics of the recently discovered multicriticality in black holes. We specifically consider black hole quadruple points in $D = 4$ Einstein gravity coupled to non-linear electrodynamics. We observe thermodynamic phase transitions between the four stable phases at a quadruple point as well as the weak and strong oscillatory phenomena by numerically solving the Smoluchowski equation describing the evolution of the probability distribution function. We analyze the dynamic evolution of the different phases at various ensemble temperatures and find that the probability distribution of a final stationary state is closely tied to the structure of its off-shell Gibbs free energy.

I. INTRODUCTION

Over the past five decades, noteworthy progress has been made in black hole thermodynamics after the four laws of black hole thermodynamics were proposed [1–5]. A particularly interesting subfield is that of critical phenomena in black hole thermodynamics. The Hawking-Page phase transition [6], which describes the transition between thermal radiation and large black holes resembling the solid-liquid phase transition, was a seminal investigation into this topic. In more recent years, the study of critical phenomena has become much better understood in the context of black hole chemistry [7], whose main idea is to treat the black hole mass as enthalpy [8], and the cosmological constant and its conjugate variable as the respective thermodynamic pressure and volume of the black hole system. Under this interpretation, there is a phase transition between large and small charged anti-de Sitter (AdS) black holes, which coincides with the gas-liquid phase transition in the Van der Waals model [9–14].

Quite recently the underlying kinetics of black hole phase transitions have been studied based on the free energy landscape model [15–18]. In this approach, black hole phase transitions can be understood to take place due to thermal fluctuations, with the black hole horizon radius regarded as the order parameter formulating the free energy landscape. The dynamic behaviour of black hole phase transitions can be understood by solving the Smoluchowski equation [19–22], which is essentially the probabilistic Fokker-Planck equation depicting the diffusion process of a system given some potential barriers. For black hole phase transitions, the effective potential barrier is described by the off-shell Gibbs free energy, which is defined as a continuous function of the black hole horizon radius at some ensemble temperature.

The discovery that black holes can have triple points has further supported the motivation for treating black holes as chemical systems [23–25]. Black hole triple points are where three stable phases – small, intermediate, and large horizon size – merge together, resembling

the triple point of water where solid, liquid, and gas coexist at a particular pressure and temperature. The dynamic behaviour of black hole triple points was recently studied [26], where initially small, intermediate, or large black holes were found to be able to transit to the other two coexistent phases at the triple point, indicating that thermodynamic phase transitions can indeed occur dynamically. Both weak and strong oscillatory behaviour were observed. In the former (weak) case, the probability of a non-initial state becomes maximal before decaying to stationarity with its probability never exceeding that of the initial state, whereas in the latter (strong) case the probability of a non-initial state exceeds that of the initial state.

Multicriticality is the most recent discovery to emerge from black hole chemistry. Multicritical points occur when several distinct phases in a system merge at a particular set of thermodynamic parameters, generalizing the notion of a triple point. A variety of settings, including 4-dimensional Einstein gravity coupled to non-linear electrodynamics [27], multiply rotating Kerr-AdS black holes [28], and spherically symmetric black holes in Lovelock gravity [29] have all been shown to have black hole solutions exhibiting multicritical behaviour. Such behaviour in black hole physics is much less understood than tricriticality and other black hole phase behaviour, and warrants further study.

Motivated by the above, we investigate the dynamic behaviour of black hole quadruple points in the context of 4-dimensional Einstein gravitational theory coupled to non-linear electrodynamics, potentially providing some insights for our understanding of the nature of black hole phase transitions. We find that the early evolution of the probability distribution of black hole phases near the quadruple point depends on the first passage time. This we find is related to the size of the Gibbs potential barrier between phases. We also find that the distribution of the final stationary phases is determined by the relative heights of the potential wells of the off-shell Gibbs free energy.

II. QUADRUPLE POINTS IN BLACK HOLE PHASE TRANSITIONS

We consider non-linear electromagnetic fields in 4-dimensional Einstein gravity. The action is given by [30]

$$S = \int d^4x [\sqrt{-g}(R - 2\Lambda - \sum_{i=1}^N \alpha_i (F^2)^i)] \quad (1)$$

where α_i are dimensional coupling constants, $F^2 = F_{\mu\nu}F^{\mu\nu}$, with the electromagnetic field tensor $F_{\mu\nu} \equiv \partial_\mu A_\nu - \partial_\nu A_\mu$, and A_μ is the electromagnetic four-potential. The sum may truncate at some finite value of N , but it is also possible to consider $N \rightarrow \infty$ (for example, as in Born-Infeld electrodynamics). The coupling constants α_i can be regarded as independent thermodynamic variables, each with their own conjugates. The existence of multicritical points depends on the relative choices of the α_i in addition to the other thermodynamic variables.

We consider the following ansatz describing spherically symmetric static black holes

$$ds^2 = -U(r)dt^2 + \frac{1}{U(r)}dr^2 + r^2d\Omega^2 \quad (2)$$

$$A_\mu = [\Phi(r), 0, 0, 0] \quad (3)$$

If the spacetime is asymptotically AdS, and Φ asymptotically vanishes, we can assume

$$\Phi = \sum_{r=1}^K b_i r^{-i} \quad U = 1 + \sum_{i=1}^K c_i r^{-i} + \frac{r^2}{l^2} \quad (4)$$

It is then possible to solve the field equations for the coefficients b_i and c_i in terms of the mass M , charge Q , and the coupling constants α_i . Any given solution depends on a finite number of parameters that can be indexed either by N (the number of α_i couplings in the action) or by K (the number of parameters in the solution), along with M and Q . In the latter case the expressions for the metric and gauge field are explicitly given by (4) whereas in the former case these expressions are determined implicitly. In either case, multicritical thermodynamic phenomena can be obtained by making appropriate choices of a finite number of α_i , with the values of K or N determining the maximal degree of multicriticality [27].

In the following context, we focus on a setting in which the α_i are nonzero and independent for $i \leq 7$; for $i \geq 8$ all remaining α_i are determined in terms of these quantities. This case is known to admit quadruple points [27]. This provides us with the simplest non-trivial example of multicritical dynamical behaviour. The solution is

$$\Phi = \frac{Q}{r} + \frac{b_5}{r^5} + \frac{b_9}{r^9} + \frac{b_{13}}{r^{13}} + \frac{b_{17}}{r^{17}} + \frac{b_{21}}{r^{21}} + \frac{b_{25}}{r^{25}} \quad (5)$$

$$U = 1 - \frac{2M}{r} + \frac{Q^2}{r^2} + \frac{b_5 Q}{2r^6} + \frac{b_9 Q}{3r^{10}} + \frac{b_{13} Q}{4r^{14}} + \frac{b_{17} Q}{5r^{18}} + \frac{b_{21} Q}{6r^{22}} + \frac{b_{25} Q}{7r^{26}} + \frac{r^2}{l^2} \quad (6)$$

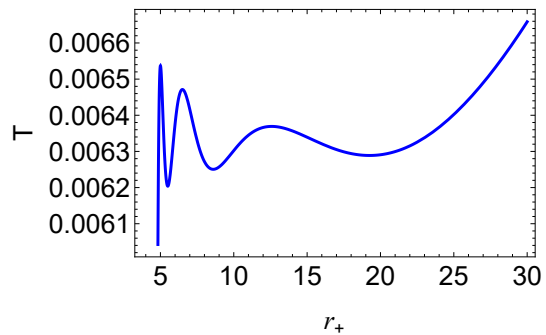


FIG. 1. Black hole quadruple points with parameters $P = 0.0000689999421$, $Q = 6.751117513$ in the T - r_+ diagram.

where the b_i are known in terms of the α_i and Q [27], and $b_i = 0$ for $i > 25$.

The thermodynamic temperature T , entropy S , pressure P , and volume V are given by

$$T = \frac{1}{4\pi r_+} \left(1 + \frac{3r_+^2}{l^2} - \frac{Q^2}{r_+^2} - 5\frac{b_5 Q}{2r_+^6} - 3\frac{b_9 Q}{r_+^{10}} - 13\frac{b_{13} Q}{4r_+^{14}} - 17\frac{b_{17} Q}{5r_+^{18}} - 7\frac{b_{21} Q}{2r_+^{22}} - 25\frac{b_{25} Q}{7r_+^{26}} \right) \quad (7)$$

$$S = \pi r_+^2, \quad P = \frac{3}{8\pi l^2}, \quad V = \frac{4\pi r_+^3}{3} \quad (8)$$

and the equation of state reads

$$P = \frac{T}{2r_+} - \frac{1}{8\pi r_+^2} + \frac{Q^2}{8\pi r_+^4} + \frac{5b_5 Q}{16\pi r_+^8} + \frac{3b_9 Q}{8\pi r_+^{12}} + \frac{13b_{13} Q}{32\pi r_+^{16}} + \frac{17b_{17} Q}{40\pi r_+^{20}} + \frac{7b_{21} Q}{16\pi r_+^{24}} + \frac{25b_{25} Q}{56\pi r_+^{28}} \quad (9)$$

where all formulae are written in Planck units, Q is the black hole charge, r_+ is the horizon radius, the size of the black hole.

The Gibbs free energy $G = M - TS$, whose global minimum as a function of T determines the thermodynamically stable state, provides a diagnostic for finding multicritical behaviour [27, 28]. The presence of $(N - 1)$ swallowtails in the $G - T$ diagram indicates N distinct phases, with the self-intersection points of the swallowtails signifying first order phase transitions between two distinct phases. Since each cusp in a swallowtail corresponds to an extremum of T as a function of r_+ , N distinct phases require $2N - 2$ distinct extrema in $T(r_+)$. If two adjacent inflections of $T(r_+)$ occur at the same temperature, then the intersection points of corresponding swallowtails will merge, yielding a tricritical point. If this occurs for $j \leq N$ different inflections, the j swallowtails will have a common self-intersection, corresponding to a j -th order multicritical point.

These critical points can be found by finely tuning the thermodynamic parameters. We can obtain a quadruple point, where the $T(r_+)$ curve has three pairs of local maxima and minima equivalently, shown in Fig.1, by

specifying

$$\begin{cases} P = 0.0000689999421 \\ Q = 6.751117513 \\ b_5 = -5078.980603 \\ b_9 = 6.054804813 \times 10^6 \\ b_{13} = -4.131510152 \times 10^9 \\ b_{17} = 1.399821234 \times 10^{12} \\ b_{21} = -2.014970449 \times 10^{14} \\ b_{25} = 1.016449472 \times 10^{16} \end{cases} \quad (10)$$

To understand the dynamics of quadruple points, we consider a canonical ensemble at some fixed temperature T_E , which is not required to be the Hawking temperature T . Under the values of the parameters we choose (10), the temperature range in which quadruple points can exist is $T_E \in (0.00628883, 0.00636918)$, as shown in Fig. 1. Regarding the horizon radius as the order parameter, we

generalize the on-shell Gibbs free energy to include black hole spacetimes with all radii. The off-shell Gibbs free energy G_L is then defined in terms of the ensemble temperature T_E instead of the Hawking temperature T , obtaining

$$\begin{aligned} G_L &= M - T_E S \\ &= \frac{1}{840r_+^{25}} (60b_{25}Q + 70b_{21}Qr_+^4 + 84b_{17}Qr_+^8 \\ &\quad + 105b_{13}Qr_+^{12} + 140b_9Qr_+^{16} + 210b_5Qr_+^{20} \\ &\quad + 420Q^2r_+^{24} + 420r_+^{26} + 1120P\pi r_+^{28}) - T_E\pi r_+^2 \end{aligned} \quad (11)$$

where M is the black hole mass (the conserved charge associated with the timelike Killing vector $\xi = \partial_t$ [27]), and S is the entropy of black hole. We see from (11) that the off-shell Gibbs free energy, as a function of r_+ , also depends on the black hole charge Q , thermodynamic pressure P , and the ensemble temperature T_E .

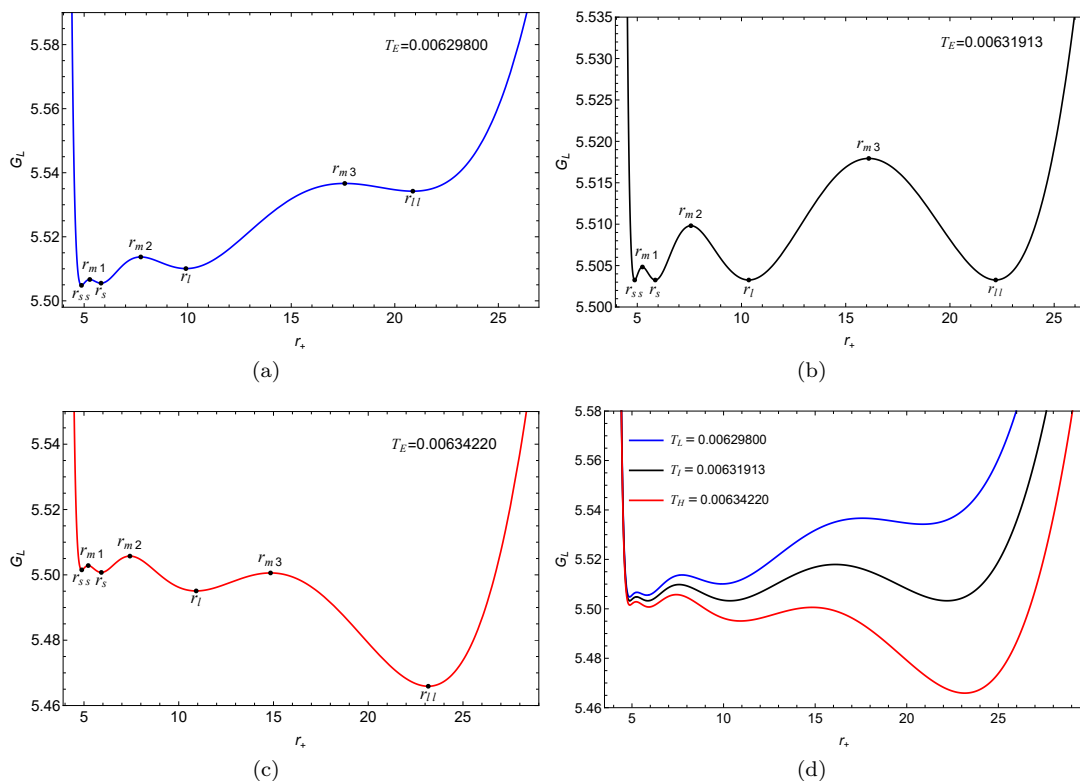


FIG. 2. Off-shell Gibbs free energy at ensemble temperatures (a) $T_E = 0.006298$, (b) $T_E = 0.00631913$, (c) $T_E = 0.0063422$. (d) Off-shell Gibbs free energy at three different ensemble temperatures are presented in one panel with low temperature $T_L = 0.006298$, intermediate temperature $T_I = 0.00631913$, and high temperature $T_H = 0.0063422$.

A union of black hole spacetimes with a range of arbitrary horizon radii constitutes the so-called black hole landscape. On this landscape, the off-shell free energy

is interpreted as the effective potential in the black hole phase transition process, and the horizon radius is regarded as the order parameter. We depict the off-shell

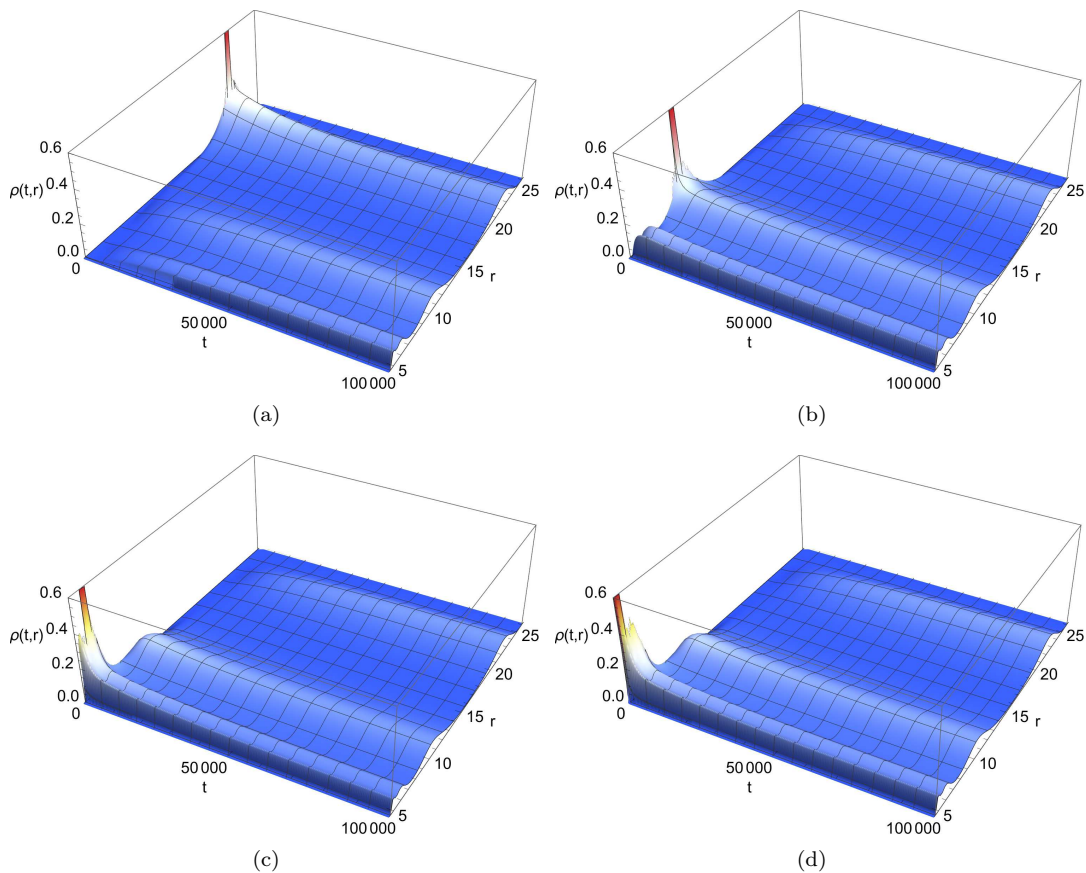


FIG. 3. Time evolution of the probability distribution $\rho(t, r)$ at middle ensemble temperature $T_E = 0.00631913$. The initial Gaussian wave packet is set to be peaked at the coexistent (a) largest (b) large (c) small and (d) smallest black hole states.

free energy G_L v.s. the horizon radius r_+ at a quadruple point with $P = 0.0000689999421$, $Q = 6.751117513$ (as given by (10)) at various ensemble temperatures, as shown in Fig. 2. Only the local extrema on the G_L curve correspond to physical black holes, which are on-shell solutions to the field equations that follow from (1). On each curve, there are four local minima, i.e. $r_k = r_{ss}$, r_s ,

r_l , and r_{ll} , representing four thermodynamic local stable black holes in order of increasing horizon size, and three local maxima, i.e. r_{m1} , r_{m2} and r_{m3} , representing three unstable black hole phases or what we call intermediate transition states. Other points on the curve denote off-shell solutions, which are transient black hole states during the phase transition process.

III. DYNAMIC PROCESSES AT THE QUADRUPLE POINT

In what follows, we shall denote the horizon radius by r for simplicity. The probability that the system will stay in a particular black hole state with horizon radius r is represented by a distribution denoted by $\rho(t, r)$. Based on the free energy landscape, black hole systems can undergo thermodynamic phase transitions and change to other black hole states through a thermal fluctuation of the order parameter r . This process can be described by the Smoluchowski equation, which is a particular case of the Fokker-Planck equation [31],

$$\frac{\partial \rho(t, r)}{\partial t} = D \frac{\partial}{\partial r} \left(e^{-\beta G_L(r)} \frac{\partial}{\partial r} \left(e^{\beta G_L(r)} \rho(t, r) \right) \right) \quad (12)$$

where $D = k_B T_E / \zeta$ is the diffusion coefficient and k_B and ζ are Boltzmann's constant and the dissipation coefficient, respectively.

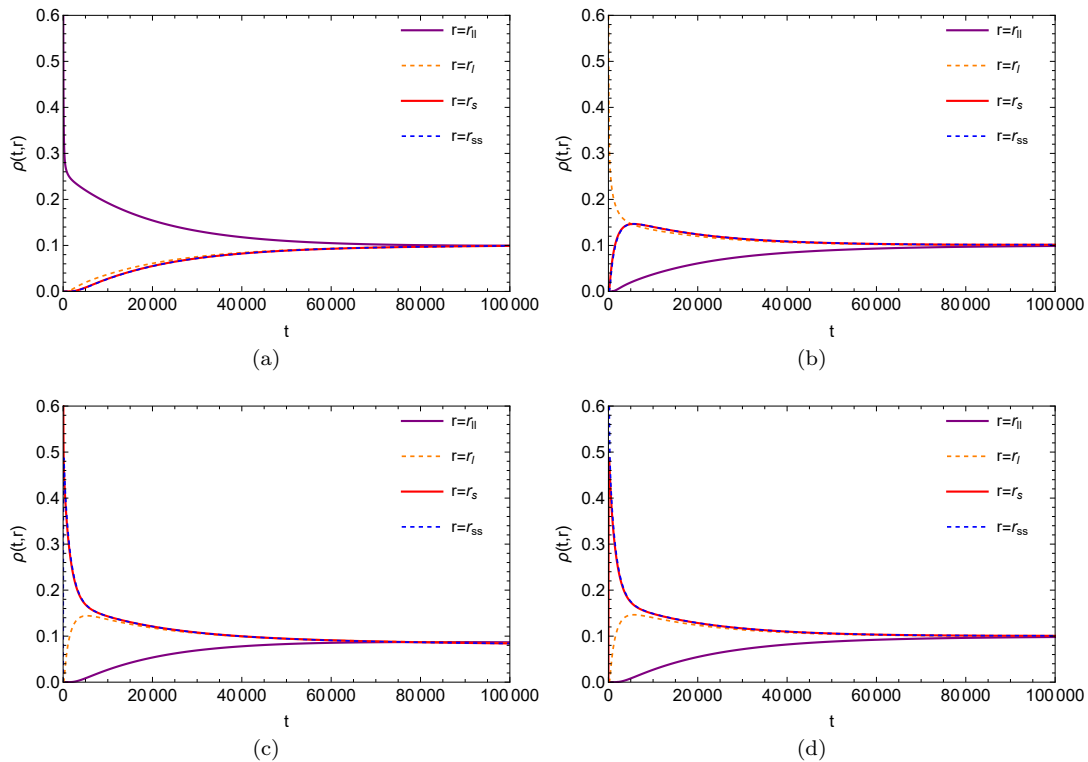


FIG. 4. Behaviours of $\rho(t, r)$ for four stable phases at middle ensemble temperature $T_E = 0.00631913$. The initial Gaussian wave packet is set to be peaked at the coexistent (a) largest (b) large (c) small and (d) smallest black hole states.

We shall use the Smoluchowski equation to study the dynamic evolution of different black hole phases at a quadruple point. Without loss of generality, we work in units where $k_B = \zeta = 1$. To solve this partial differential equation, we need to impose both initial conditions and boundary conditions. For initial conditions, we set the initial state to be some Gaussian wave packet

$$\rho(0, r) = \frac{1}{\sigma\sqrt{\pi}} e^{-\frac{(r-r_i)^2}{\sigma^2}} \quad (13)$$

peaked at the horizon radius r_i corresponding to one of the four distinct stable black hole phases.

We numerically set $\sigma = 0.2$ and consider the initial state to be respectively peaked at the coexistent black hole state with smallest, small, large, and largest horizon radius, i.e. $r_i = r_{ss}, r_s, r_l$, or r_u . We impose reflective boundary conditions at $r = 0$ and $r = \infty$, where there are extremely high potential barriers

$$e^{-\beta G_L(r)} \frac{\partial}{\partial r} \left(e^{\beta G_L(r)} \rho(t, r) \right) \Big|_{r=r_{bdy}} = 0 \quad (14)$$

to ensure that the total probability is preserved over time.

We numerically choose the left boundary and right boundary to be at $r = 1$ and $r = 30$ to solve the Smoluchowski equation. The final stationary probability distributions, $\rho(t, r)$ should not depend on time (the probability current must vanish), so the final state probability distributions $\rho(r) \propto e^{-\beta G_L(r)}$ must only depend on the structure of Gibbs free energy, which is determined by the ensemble temperature.

We consider the behaviour of G_L for three distinct values of the ensemble temperature T_E , shown in Fig. 2. At the intermediate ensemble temperature (Fig. 2(b)) the four local minima representing four stable states in the Gibbs free energy diagram share the same value $G_L = 5.50326$. For a slightly smaller value of T_E (Fig. 2(a)) the minima are no longer degenerate, and instead increase from r_{ss} to r_u . For a slightly larger value of T_E (Fig. 2(c)) the minima decrease from r_{ss} to r_u .

A. Intermediate Ensemble Temperature

We plot in Fig. 3 the behaviour of the probability distribution ρ as a function of (t, r) , for initial states peaked

at each of the $r_i = r_u, r_l, r_s$, and r_{ss} . In Fig. 4 we plot for

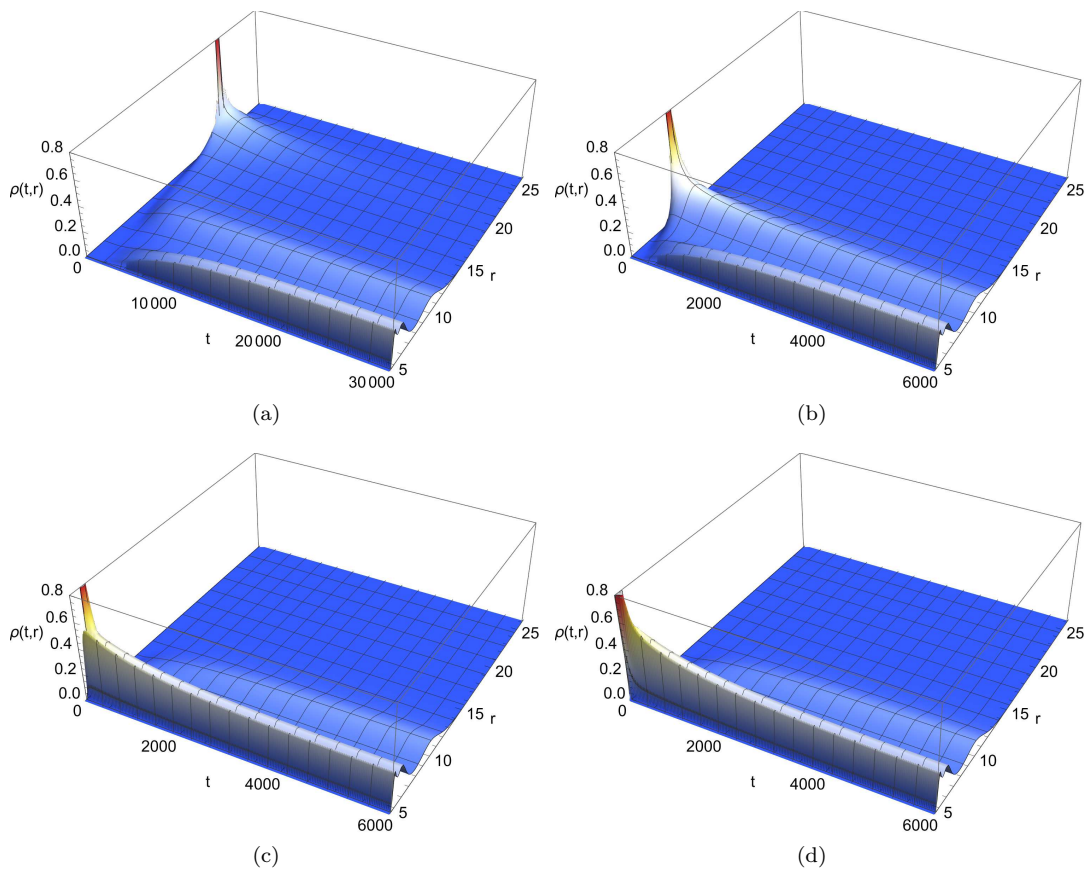


FIG. 5. Time evolution of the probability distribution $\rho(t, r)$ at low ensemble temperature $T_E = 0.006298$. The initial Gaussian wave packet is set to be peaked at the coexistent (a) largest (b) large (c) small and (d) smallest black hole states.

each of these successive cases the evolution of ρ at each of the values $r_i = r_{ss}, r_s, r_l$, and r_U .

Consider the first case, shown in Fig. 3(a) and Fig. 4(a), in which the probability is initially peaked at the black hole state with largest horizon radius, which means $\rho(0, r_U) \gg \rho(0, r_l) \approx \rho(0, r_s) \approx \rho(0, r_{ss}) \approx 0$. As time increases, there is a decline of the probability of the largest phase (with radius r_U), whilst the probabilities of the other three phases gradually increase. Note that in this process $\rho(t, r_l) > \rho(t, r_s) > \rho(t, r_{ss})$ with $\rho(t, r_s) \approx \rho(t, r_{ss})$. This is because the off-Shell Gibbs free energy, interpreted as a potential, has more barriers between the largest and the two smallest black hole phases, with radii r_s and r_{ss} than the phase with radius r_l . The reason that $\rho(t, r_s) \approx \rho(t, r_{ss})$ is that the barrier width (defined as the separation between a minimum and the adjacent maximum) and height is relatively small between these two black hole states. After a sufficiently long time, say $t > 100000$, the four states equilibrate to the multicritical state, sharing the same probability $\rho(r_k, t) \approx 0.1$, for $k = ll, l, s$ and ss , due to the degener-

ate local minima value in the Gibbs free energy diagram Fig. 2(b).

Consider the next case shown in Fig. 3(b) and 4(b), in which the initial wave packet is set to be located at the large black hole state with radius r_l . At the beginning, we have $\rho(0, r_l) \gg \rho(0, r_U) \approx \rho(0, r_s) \approx \rho(0, r_{ss}) \approx 0$. At early times, the probability of the phase with large radius declines rapidly, whilst $\rho(t, r_U), \rho(t, r_s)$, and $\rho(t, r_{ss})$ increase. It is noteworthy that the probability leakage to the small and smallest black hole states grows much faster than that to the largest state. This is due to the relatively small potential barrier heights and widths between the large state and the two smallest states. The probabilities $\rho(t, r_s)$, and $\rho(t, r_{ss})$ quickly reach their maximal values, which are even (slightly) larger than the probability $\rho(t, r_l)$ of the given initial state. This signifies a change of dominant state, in this case from the large phase to the small and smallest black hole phases. This phenomenon is called strong oscillatory behaviour [26]. At the end, the four probabilities become stationary and equilibrate to almost the same value, as expected due to the structure of G_L .

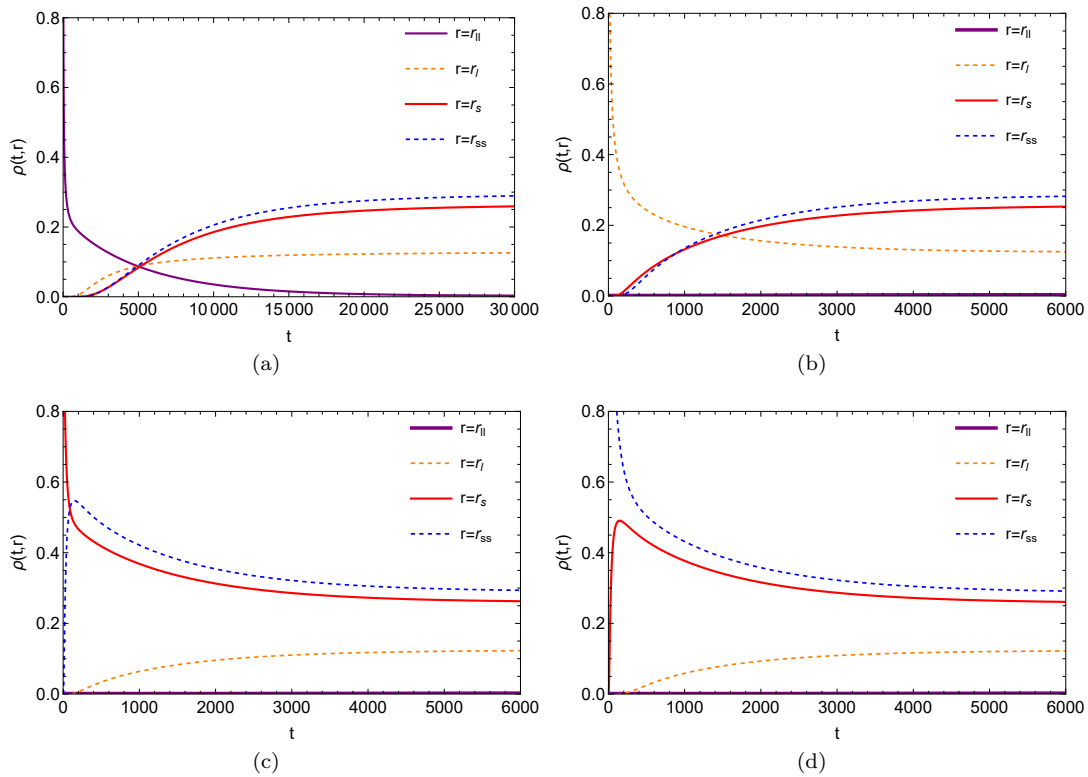


FIG. 6. Behaviours of $\rho(t, r)$ for four stable phases at low ensemble temperature $T_E = 0.006298$. The initial Gaussian wave packet is initialized to peak at the coexistent (a) largest (b) large (c) small and (d) smallest black hole states.

Turning now to the remaining two cases, consider the initial wave packet peaked at $r = r_s$, as shown in Fig. 3(c) and Fig. 4(c). At early times, the probability leaks from $\rho(t, r_s)$ to $\rho(t, r_{ss})$ very quickly since the potential barrier width and height between the small and smallest black hole states are extremely small. After a short time, the probability curves for the small and smallest black hole phases almost overlap. The probability $\rho(t, r_l)$ for the large phase grows to a maximum value smaller than that of $\rho(t, r_s)$ and $\rho(t, r_{ss})$, then decreases to the stationary value. This phenomenon is called weak oscillatory behaviour [26]. In the evolution process, $\rho(t, r_u)$ for the largest black hole state has the lowest value and grows the slowest. This is because the largest phase is the furthest away from the initial state.

Finally, if the distribution is peaked at the smallest phase (Fig. 4(d)), the behaviour of all four curves resembles those of Fig. 4(c), the only distinction being that the roles $\rho(t, r_s)$ and $\rho(t, r_{ss})$ play are interchanged.

B. Low and High Ensemble Temperatures

For low ensemble temperature $T_E = 0.006298$, shown in Fig. 2(a), the key feature of the off-shell Gibbs free

energy is $G_L(r_{ss}) < G_L(r_s) < G_L(r_l) < G_L(r_u)$. Hence the smallest black hole phase will be the final dominant state regardless of the given initial state, with the final stationary state probability distributions being $\rho(t, r_{ss}) > \rho(t, r_s) > \rho(t, r_l) > \rho(t, r_u)$, as shown in Fig. 5 and Fig. 6. So we observe strong oscillatory phenomena when the initial state is peaked at r_u , r_l , and r_s , as respectively shown in Fig. 6(a), Fig. 6(b), and Fig. 6(c), while Fig. 6(d) exhibits weak oscillatory behaviour. The final probability for the largest black hole state is extremely small compared to the other three states due to its largest Gibbs free energy value. The final probability distributions $\rho(t, r_{ss})$ and $\rho(t, r_s)$ are relatively approximate due to the smallest barrier size between these two states. More structures can be viewed with more discernment. For instance, as depicted in Fig. 6(a), the large black hole phase probability grows faster than that of the small and smallest black hole phases at early times, since the large black hole phase is closer to the initial state peaked at r_u . But the lower free energy of phases at $r = r_s$ and $r = r_{ss}$ reverses the situation after $t \approx 5000$.

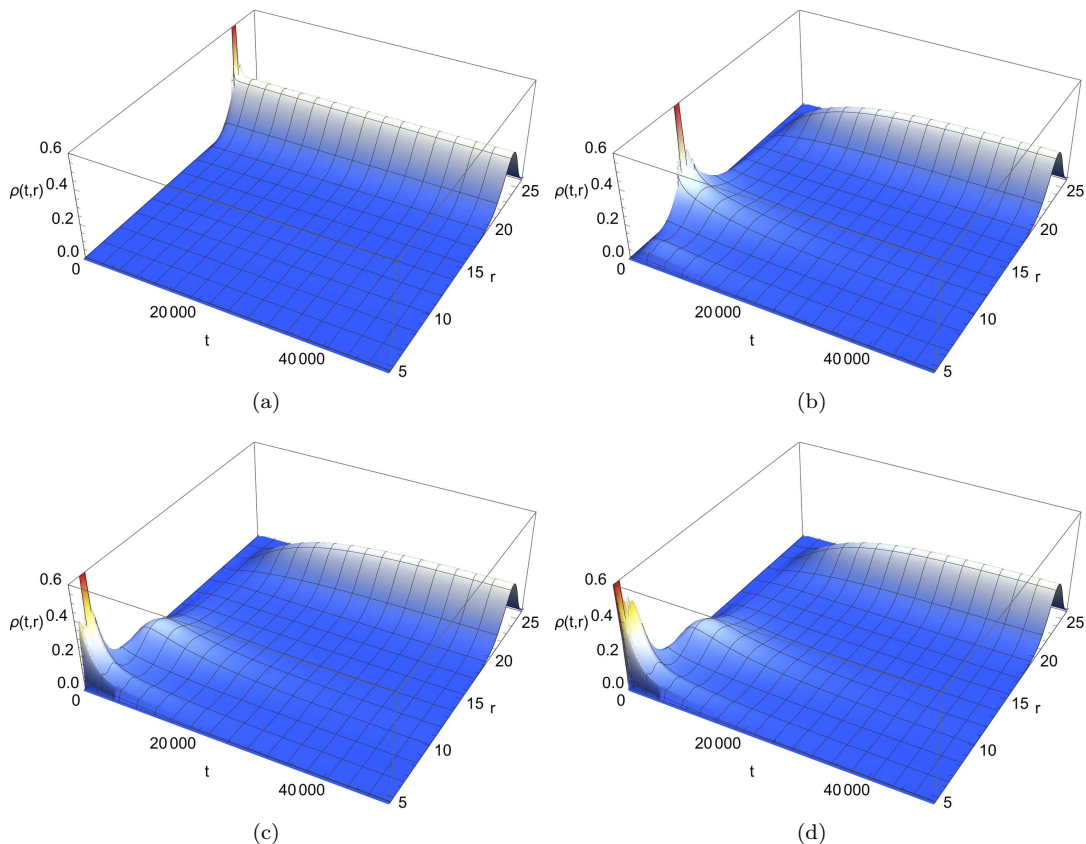


FIG. 7. Time evolution of the probability distribution $\rho(t, r)$ at high ensemble temperature $T_E = 0.0063422$. The initial Gaussian wave packet is initialized to peak at the coexistent (a) largest (b) large (c) small and (d) smallest black hole states.

For high ensemble temperature $T_E = 0.0063422$, shown in Fig. 2(c), note that $G_L(r_{ss}) > G_L(r_s) > G_L(r_l) > G_L(r_u)$ in the $G_L - r_+$ diagram, and the barrier height and width to transit from the largest black hole state with radius r_u to the other three states is extremely large. Hence, regardless of the given initial state, the largest black hole phase is eventually dominant, as shown in Fig. 7. Its final probability is much larger than the other three phases, with the final stationary states probability distribution $\rho(t, r_u) \gg \rho(t, r_l) > \rho(t, r_s) > \rho(t, r_{ss})$, illustrated in Fig. 8. That is why strong oscillatory phenomena are observed in Fig. 8(b), Fig. 8(c), and Fig. 8(d). Taking a closer look at Fig. 8(b), initially $\rho(t, r_l)$ leaks to other three states and $\rho(t, r_s) \gtrsim \rho(t, r_{ss}) > \rho(t, r_u)$ because the barrier widths amongst r_s, r_{ss} and r_l are much smaller than that between r_u and r_l . Afterward $\rho(t, r_{ss}) \approx \rho(t, r_s) < \rho(t, r_u)$ due to the lowest Gibbs value at $r = r_u$. Similar behaviours can be observed in Fig. 8(c), and Fig. 8(d). Hence, in the early stage, barrier widths and heights play an important role in the evolution process, whereas in the later stage, the value of the Gibbs free energy becomes crucial.

IV. THE FIRST PASSAGE EVENTS AT DIFFERENT ENSEMBLE TEMPERATURES

In this section, we investigate the underlying reasons for black hole phase transition behaviours at quadruple points by inspecting the first passage events. On the free energy landscape, the first passage time for a given initial phase describes the required time to first ascend to the top of nearby the free energy barriers that correspond to unstable phases. Reflecting boundary conditions are still imposed at $r = 0$ and $r = \infty$, and to depict the first passage event we impose absorbing boundary conditions at r_{m1}, r_{m2} , and r_{m3} for each unstable state:

$$\rho(t, r_{m1}) = \rho(t, r_{m2}) = \rho(t, r_{m3}) = 0 \quad (15)$$

Focusing on the Intermediate ensemble temperature shown in Fig.3(a), let us denote the first passage time distributions by $F_{p1}(t)$, $F_{p2}(t)$, $F_{p3}(t)$ and $F_{p4}(t)$ for the 4 initial cases $r_i = r_{ss}, r_s, r_l$, and r_u , respectively. Applying the

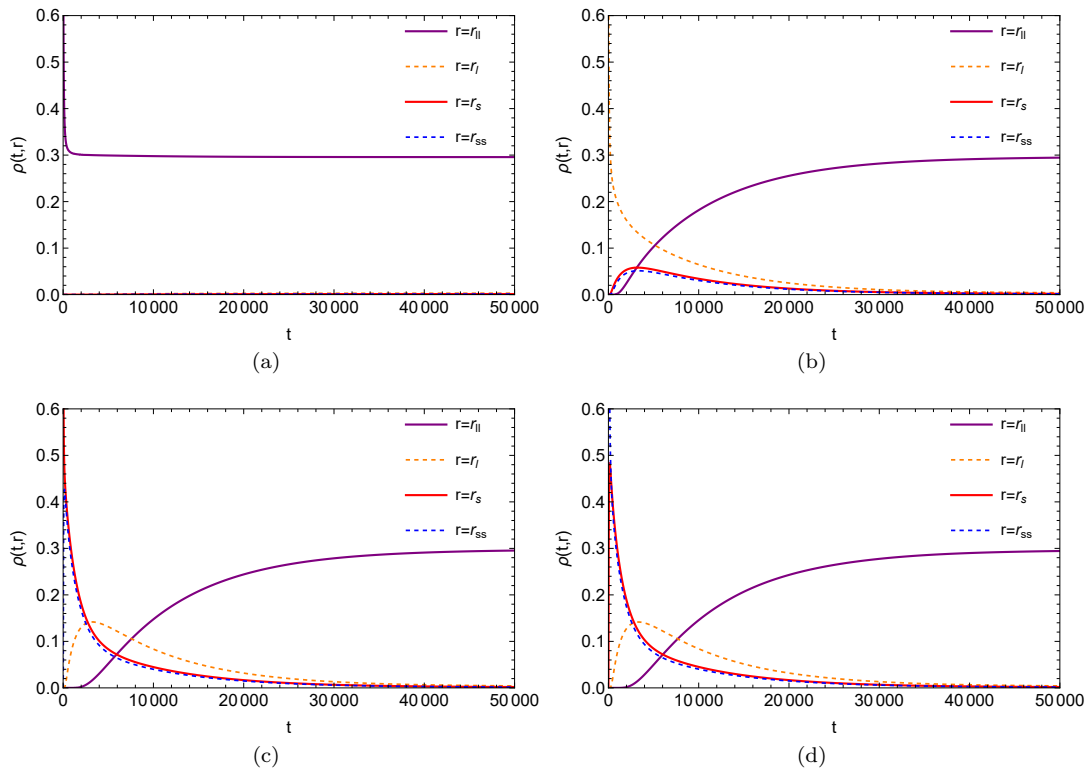


FIG. 8. Behaviours of $\rho(t, r)$ for four stable phases at the high ensemble temperature $T_E = 0.0063422$. The initial Gaussian wave packet is set to be peaked at the coexistent (a) largest (b) large (c) small and (d) smallest black hole states.

Smoluchowski equation and boundary conditions, the first passage time distributions are expressed as

$$F_{p1}(t) = -\frac{\partial \rho(t, r_{m1})}{\partial r}, \quad (16)$$

$$F_{p2}(t) = \frac{\partial \rho(t, r_{m1})}{\partial r} - \frac{\partial \rho(t, r_{m2})}{\partial r}, \quad (17)$$

$$F_{p3}(t) = \frac{\partial \rho(t, r_{m2})}{\partial r} - \frac{\partial \rho(t, r_{m3})}{\partial r}, \quad (18)$$

$$F_{p4}(t) = \frac{\partial \rho(t, r_{m3})}{\partial r}. \quad (19)$$

We plot the first passage time distribution at three different ensemble temperatures, as shown in Fig. 9, Fig. 10, and Fig. 11. For each first passage time distribution curve, $F_p(t)$ reaches a peak after a short time and then decays rapidly. This indicates there is a large probability that the first passage event occurs in a very short time. This provides us with information for understanding the behaviour of $\rho(t, r)$ at early times.

In Table I, we list the height and width of each barrier at the three different ensemble temperatures. At each temperature, we find the extreme point t of the first passage time distribution for each case and list these values in Table II. The differences amongst the various barrier widths are larger than the differences amongst the barrier heights, so barrier widths are more crucial in determining transit behaviour. We therefore use barrier width W to label the barrier size in the following context. What we conclude from Table I and Table II is that the time corresponding to the peak of the first passage time distribution t is highly correlated with barrier size.

Consider, for example, the intermediate temperature T_I and high temperature T_H . From t_{I13} to t_{SS1} , the first passage time peak t decreases, i.e., $t_{I13} > t_{I12} > t_{I2} > t_{S2} > t_{S1} > t_{SS1}$, and we have $W_{I13} > W_{I12} > W_{I2} > W_{S2} > W_{S1} > W_{SS1}$ – it is easier to surmount a barrier with small width. Likewise at low temperature T_L , we have $t_{L13} > t_{L12} > t_{L2} > t_{S2} > t_{S1} > t_{SS1}$, with corresponding barrier widths $W_{L13} > W_{L12} > W_{L2} > W_{S2} > W_{S1} > W_{SS1}$. The interchange of the largest first passage time is accompanied by an interchange of the largest barrier width.

To explain the dynamic behaviour of multicritical black hole phase transitions at early times, we make the assumption that the time needed from the barrier top to reach the adjacent local minimum is much shorter than the first passage time to climb to the barrier top from the initial local stable state [16]. Thus we obtain the first passage time

scales from each initial black hole state to other stable states, symbolizing the difficulty of transitioning from one stable phase to another, as shown in Table III. Let us focus on the intermediate ensemble temperature $T_E = 0.00631913$. First, for the initial black hole state with the largest horizon radius r_{ll} , we have $t(ll \rightarrow l) < t(ll \rightarrow s) \lesssim t(ll \rightarrow ss)$ ($1593 < 1817 \lesssim 1827$), which means that it is easier for the probability to leak to the state with radius r_l . This is why in Fig. 4(a), we observe the phenomenon that $\rho(t, r_l) > \rho(t, r_s) \gtrsim \rho(t, r_{ss})$ at early times. For a large initial black hole state with radius r_l , we have the early time behaviour $\rho(t, r_s) \gtrsim \rho(t, r_{ss}) > \rho(t, r_{ll})$ shown in Fig. 4(b), which we can understand from the phase transition time scale relations $t(l \rightarrow s) \lesssim t(l \rightarrow ss) < t(l \rightarrow ll)$. For a small initial black hole state, shown in Fig. 4(c), we find that $t(s \rightarrow ss) < t(s \rightarrow l) < t(s \rightarrow ll)$, explaining why $\rho(t, r_{ss})$ is initially the fastest-growing probability and $\rho(t, r_{ll})$ the slowest, with $\rho(t, r_{ss}) > \rho(t, r_l) > \rho(t, r_{ll})$. Similarly, if the initial state is the smallest black hole, shown in Fig. 4(d), the reason why $\rho(t, r_s) > \rho(t, r_l) > \rho(t, r_{ll})$ at early times is that $t(ss \rightarrow s) < t(ss \rightarrow l) < t(ss \rightarrow ll)$.

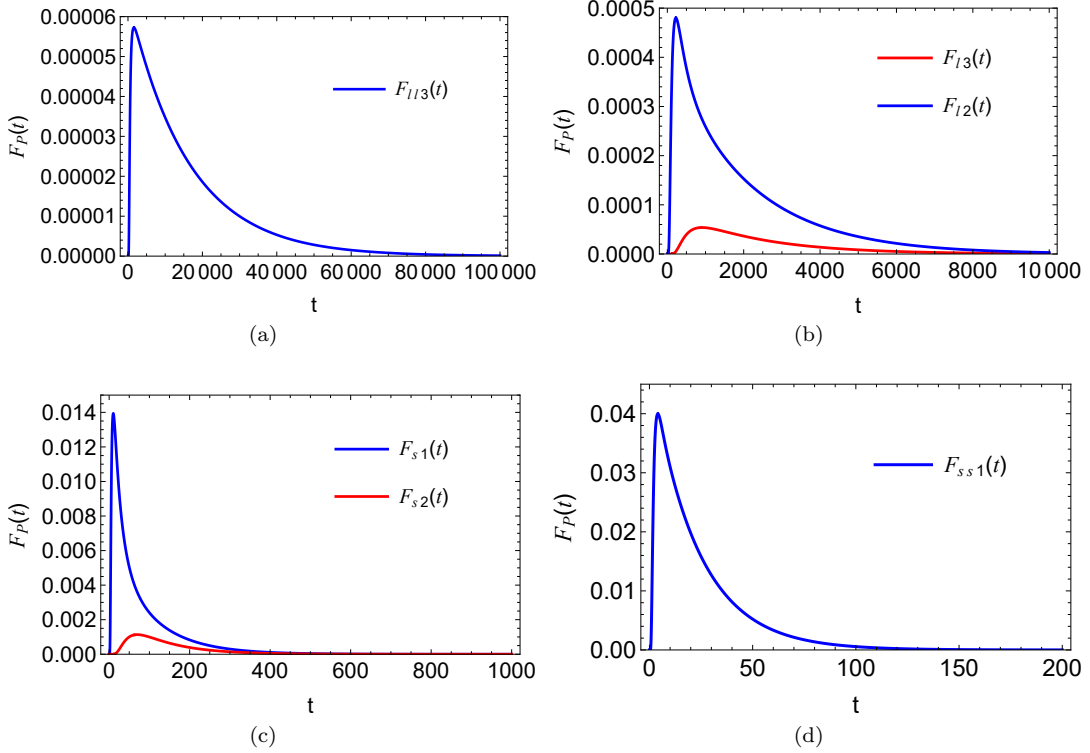


FIG. 9. First passage time distribution at intermediate ensemble temperature $T_E = 0.00631913$ for initial (a)largest, (b) large, (c) small, (d) smallest black hole respectively.

Let us examine the low ensemble temperature case with $T_E = 0.006298$, whose Gibbs free energy structure is given by Fig. 2(a). When starting with the initial black hole state peaked at the largest horizon radius r_{ll} , shown in Fig. 6(a), the probability is more likely to leak to the state with radius r_l at early times; we observe that $\rho(t, r_l) > \rho(t, r_s) \gtrsim \rho(t, r_{ss})$, which is consistent with the relation $t(ll \rightarrow l) < t(ll \rightarrow s) \lesssim t(ll \rightarrow ss)$. However, the situation reverses at late times: from Fig. 6(a) we observe that $\rho(t, r_{ll}) < \rho(t, r_l) < \rho(t, r_s) < \rho(t, r_{ss})$. This is because the Gibbs free energy has the relation $G_L(r_{ss}) < G_L(r_s) < G_L(r_l) < G_L(r_{ll})$ at low ensemble temperature, and the final state probability distributions $\rho(r) \propto e^{-\beta G_L(r)}$, which means states with lower free energy have a higher probability of being occupied. The different orderings of the probability distributions for the states with the four stable horizon radii in the early and late stages result in the intersection points of these curves in Fig. 6(a), which we call strong oscillatory behaviour. For the large initial black hole state with radius r_l , Fig. 6(b) shows that $\rho(t, r_s) \gtrsim \rho(t, r_{ss}) \gg \rho(t, r_{ll})$ at early times, owing to the phase transition time scale relationship $t(l \rightarrow s) \lesssim t(l \rightarrow ss) < t(l \rightarrow ll)$. The probability distribution function $\rho(t, r)$ for the initial small black hole in Fig. 6(c) exhibits the fastest growth rate at r_{ss} and the slowest growth rate at r_{ll} during the early stages of evolution. Specifically, we observe that $\rho(t, r_{ss}) > \rho(t, r_l) > \rho(t, r_{ll})$, which can be attributed to the ordering $t(s \rightarrow ss) < t(s \rightarrow l) < t(s \rightarrow ll)$ of the transition time scales. Similarly, for the initial state with the smallest black hole in Fig. 6(d), we find that $\rho(t, r_s)$ grows the fastest at early times, followed by $\rho(t, r_l)$

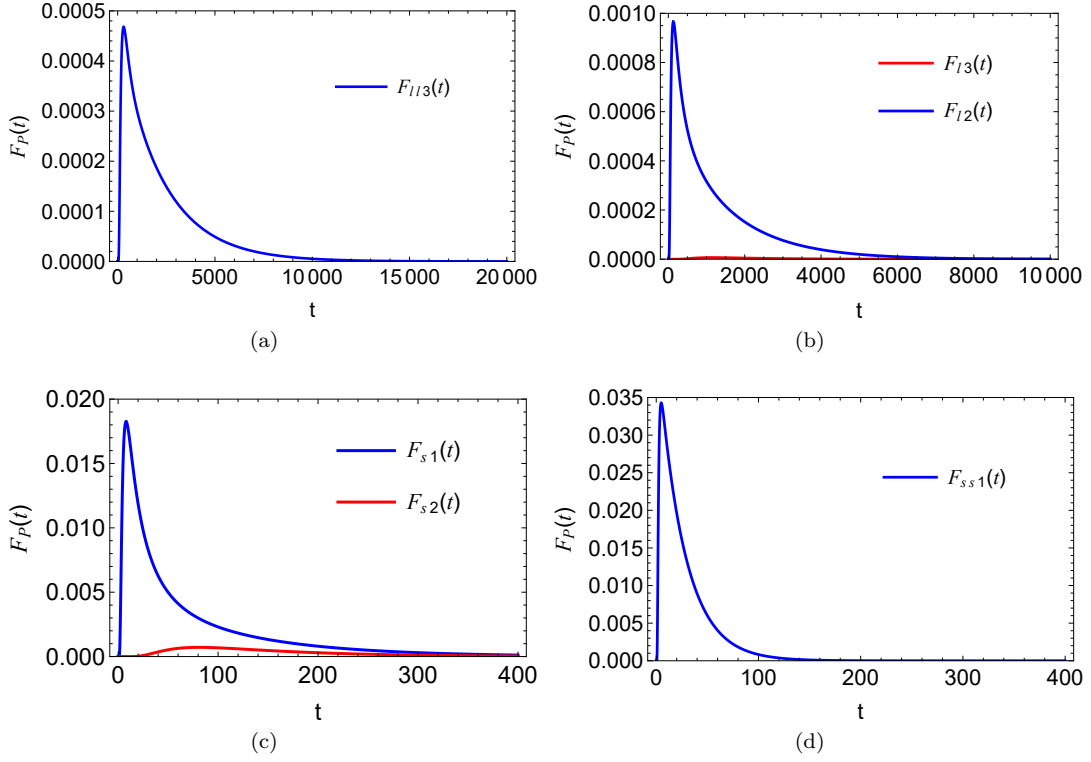


FIG. 10. First passage time distribution at low ensemble temperature $T_E = 0.006298$ for initial (a) largest, (b) large, (c) small, (d) smallest black hole respectively.

	H_{ll3}	H_{l3}	H_{l2}	H_{s2}	H_{s1}	H_{ss1}
T_L	0.0024	0.027	0.0036	0.0082	0.0011	0.0018
T_I	0.015	0.015	0.0066	0.0066	0.0016	0.0016
T_H	0.035	0.0055	0.011	0.0050	0.0021	0.0013
	W_{ll3}	W_{l3}	W_{l2}	W_{s2}	W_{s1}	W_{ss1}
T_L	3.3	7.7	2.2	1.9	0.54	0.40
T_I	6.1	5.8	2.8	1.7	0.62	0.37
T_H	8.3	3.9	3.5	1.5	0.69	0.34

TABLE I. Barrier height H and barrier width W from initial largest ($r = r_{ll}$), large ($r = r_l$), small ($r = r_s$) and smallest ($r = r_{ss}$) black hole states to the adjacent top of the barrier $r = r_{m1}$, $r = r_{m2}$, and $r = r_{m3}$.

and $\rho(t, r_{ll})$, consistent with the order of time scales for transitions: $t(ss \rightarrow s) < t(ss \rightarrow l) < t(ss \rightarrow ll)$. And for the final states in Fig. 6(b), Fig. 6(c), and Fig. 6(d), we observe the same phenomenon as Fig. 6(a), $\rho(t, r_{ll}) < \rho(t, r_l) < \rho(t, r_s) < \rho(t, r_{ss})$, which is determined only by the structure of the Gibbs free energy in Fig. 2(a) and is independent of the initial state. Similarly, at high ensemble temperature $T_E = 0.0063422$, the dynamic behaviours at early times shown in Fig. 8 can also be explained well utilizing the first passage time presented in Table III, while the late time behaviour is governed by the off-shell Gibbs free energy, shown in Fig. 2(c).

We now study the impact of ensemble temperatures on first passage events. Our findings, presented in Table I and Table II, indicate that as the ensemble temperature rises, the barrier widths for W_{ll3} , W_{l2} , W_{s1} increase, resulting

	t_{ll3}	t_{l3}	t_{l2}	t_{s2}	t_{s1}	t_{ss1}
T_L	307	1160	132	81	8	5
T_I	1593	912	224	70	10	4
T_H	3309	466	363	58	13	3

TABLE II. First passage time peak from initial largest ($r = r_{ll}$), large ($r = r_l$), small ($r = r_s$) and smallest ($r = r_{ss}$) black hole states to the adjacent top of the barrier $r = r_{m1}$, $r = r_{m2}$, and $r = r_{m3}$.

	$t(l \rightarrow l)$	$t(l \rightarrow s)$	$t(l \rightarrow ss)$
T_L	307	439	447
T_I	1593	1817	1827
T_H	3309	3672	3685
	$t(l \rightarrow s)$	$t(l \rightarrow ss)$	$t(l \rightarrow ll)$
T_L	132	140	1160
T_I	224	234	912
T_H	363	376	466
	$t(s \rightarrow ss)$	$t(s \rightarrow l)$	$t(s \rightarrow ll)$
T_L	8	81	1241
T_I	10	70	982
T_H	13	58	524
	$t(ss \rightarrow s)$	$t(ss \rightarrow l)$	$t(ss \rightarrow ll)$
T_L	5	86	1246
T_I	4	74	986
T_H	3	61	527

TABLE III. First passage time scale from initial largest ($r = r_{ll}$), large ($r = r_l$), small ($r = r_s$) and smallest ($r = r_{ss}$) black hole states to other stable states.

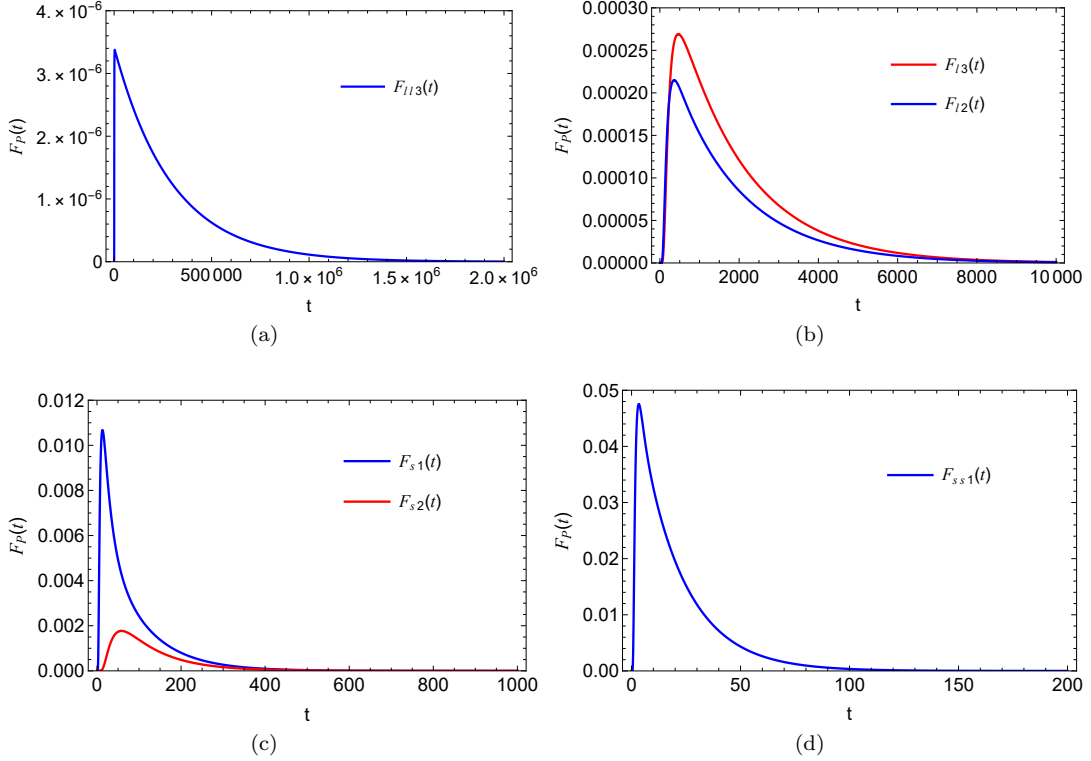


FIG. 11. First passage time distribution at high ensemble temperature $T_E = 0.0063422$ for initial (a)largest, (b) large, (c) small, (d) smallest black hole respectively.

in an increase for the respective first passage times t_{ll3}, t_{l2}, t_{s1} . Conversely, higher temperatures cause a decrease in W_{l3}, W_{s2}, W_{ss1} , leading to a decline in t_{l3}, t_{s2}, t_{ss1} . This provides further evidence that there is a positive correlation between the peak time of first passage time distribution and barrier width. Specifically, we see from Fig. 2 that a change in temperature does not substantively change the size of the barrier between the smallest and small phases, whereas the barrier between the large and largest phases undergoes a huge change. Consider then the cases where the initial state is peaked at the largest black hole states at different ensemble temperatures. The first passage times to reach the state with radius r_l from r_{ll} are denoted by F_{ll3} . As shown in Fig. 2, when the ensemble temperature increases, both barrier height and barrier width increase for the initial largest black hole. Comparing Fig. 10(a), Fig. 9(a), and Fig. 11(a), we conclude that as temperature increases, the peak of the first passage time distributions

moves rightward and becomes smaller, indicative of the increasing difficulty to surmount higher and wider barriers. Computing the first passage times, we have $t_{l3}=307, 1593, 3309$ for low, intermediate, and high ensemble temperature T_E , respectively. Notably, a significantly long time is needed to reach other states from the largest black hole state at high temperatures. The drastically low value of F_{l3} and long first passage time explain the final predominance of the largest black hole state at high temperatures.

V. CONCLUSIONS

Studying black hole thermodynamics and phase transitions offers valuable insights into the microscopic structure of black holes. We have carried out the first investigation of the dynamical behaviour of a multicritical phase transition, concentrating specifically on black hole quadruple points in Einstein gravity coupled to non-linear electrodynamics. The quadruple point is characterized by three pairs of local maxima and minima on a T - r_+ phase diagram whose inflection points are all at the same temperature T , corresponding to the temperature at multicriticality. On the free energy landscape, with G_L as potential and r_+ as the order parameter, there are four potential wells for quadruple points, representing four coexisting black hole phases.

To study the multicritical phase transition dynamics, we set the initial state to be one of the four stable black hole phases, employing the Smoluchowski equation to solve for the evolution of the probability distribution. We find that the probability density of the initial state diffuses to the other three states, with the diffusion rate depending on the first passage time distribution. We find that this distribution in turn is governed by the size of the potential barriers between the states in the off-shell Gibbs free energy. The probability distribution stabilizes at late times, and the probabilities of the four phases are determined by the values of the off-shell Gibbs free energy.

The first passage time distribution has a characteristic pattern where it rapidly rises to a peak within a short time and then quickly declines, indicating that there is a high probability of the first passage event occurring within a short time period. The shorter the corresponding first passage time, the greater the probability density of the initial state diffusing to an adjacent phase.

The different orderings of the $\rho(t, r)$ of the four phases at early and late times result in strong oscillatory phenomena: for example (Fig. 6(a)), at early times, $\rho(t, r_u) > \rho(t, r_l) > \rho(t, r_s) \gtrsim \rho(t, r_{ss})$, whereas at late times the situation reverses, and $\rho(t, r_u) < \rho(t, r_l) <$

$\rho(t, r_s) < \rho(t, r_{ss})$. The different orderings of the probability distributions for the states with the four stable horizon radii in the early and late stages result in the intersection points of these curves in Fig. 6(a), which is strong oscillatory behaviour.

Additionally, even with the same orderings, there may exist weak oscillatory phenomena. And orderings of the $\rho(t, r)$ are affected by G_L . Thus, the evolution of black hole states at the quadruple point is actually determined by the structure of the off-shell Gibbs free energy diagram. We have found that temperature is an important factor that can alter the structure of the off-shell Gibbs free energy diagram, and therefore it also affects black hole phase transitions.

Our results extend previous work carried out for black hole triple point phase transitions [26]. We have concentrated on investigating the dynamic behaviours of the quadruple point under varying ensemble temperatures, showing how these influence the probability distributions in a multiphase scenario. By analyzing the initial diffusion and final stable behaviours of the four stable states, we explain the oscillatory behaviours observed during the evolution process.

In conclusion, we investigate intriguing phenomena of black hole phase transitions from the perspective of stochastic dynamics. This study may help to understand the underlying physics of black hole phase transitions and the microscopic structure of black holes. Additionally, the free energy landscape model can also be used to examine the dynamic behaviours of the quintuple points or higher multicritical points [27–29], where more complex behaviour may become manifest.

Acknowledgements.—We would like to thank Jerry Wu, Si-Jiang Yang, Shao-Wen Wei, Yu-Xiao Liu, Yong-Qiang Wang, and Niayesh Afshordi for helpful discussions. This work was supported in part by the Natural Sciences and Engineering Research Council of Canada. J.Y. is grateful for support from a Mitacs Globalink Graduate Fellowship and encouragements from Hai-jun Wang and Han-qing Liu.

-
- [1] S. W. Hawking, *Nature* **248** (1974), 30-31
 - [2] S. W. Hawking, *Commun. Math. Phys.* **43**, 199 (1975).
 - [3] J. D. Bekenstein, *Lett. Nuovo Cim.* **4** (1972), 737-740
 - [4] J. D. Bekenstein, *Phys. Rev. D* **7**, 2333 (1973).
 - [5] J. M. Bardeen, B. Carter, and S. Hawking, *Commun. Math. Phys.* **31**, 161 (1973).
 - [6] S. W. Hawking and D. N. Page, *Commun. Math. Phys.* **87**, 577 (1983)
 - [7] D. Kubiznak, R. B. Mann and M. Teo, *Class. Quant. Grav.* **34**, no.6, 063001 (2017), [arXiv:1608.06147 [hep-th]].
 - [8] D. Kastor, S. Ray, and J. Traschen, *Class. Quant. Grav.* **26**, 195011 (2009), [arXiv:0904.2765 [hep-th]].
 - [9] D. Kubiznak and R. B. Mann, *J. High Energy Phys.*

- 1207**, 033 (2012), [arXiv:1205.0559 [hep-th]].
- [10] X. N. Wu, Phys. Rev. D **62** (2000), 124023
- [11] R.-G. Cai, L.-M. Cao, L. Li, and R.-Q. Yang, J. High Energy Phys. **1309**, 005 (2013), [arXiv:1306.6233[gr-qc]].
- [12] B. P. Dolan, Class. Quant. Grav. **28** (2011), 235017 [arXiv:1106.6260 [gr-qc]].
- [13] A. Chamblin, R. Emparan, C. V. Johnson and R. C. Myers, Phys. Rev. D **60** (1999), 064018 doi:10.1103/PhysRevD.60.064018 [arXiv:hep-th/9902170 [hep-th]].
- [14] A. Chamblin, R. Emparan, C. V. Johnson and R. C. Myers, Phys. Rev. D **60** (1999), 104026 doi:10.1103/PhysRevD.60.104026 [arXiv:hep-th/9904197 [hep-th]].
- [15] R. Li, and J. Wang, Phys. Rev. D **102**, 024085 (2020).
- [16] R. Li, K. Zhang, and J. Wang, J. High Energy Phys. **2010**, 090 (2020), [arXiv:2008.00495 [hep-th]].
- [17] R. Li and J. Wang, Nucl. Phys. B **976** (2022), 115714 [arXiv:2012.05424 [gr-qc]].
- [18] R. Li, K. Zhang and J. Wang, Phys. Rev. D **104** (2021) no.8, 084076 [arXiv:2102.09439 [gr-qc]].
- [19] S. W. Wei, Y. X. Liu and Y. Q. Wang, Nucl. Phys. B **976** (2022), 115692 doi:10.1016/j.nuclphysb.2022.115692 [arXiv:2009.05215 [gr-qc]].
- [20] S. J. Yang, R. Zhou, S. W. Wei and Y. X. Liu, Phys. Rev. D **105** (2022) no.8, 8 doi:10.1103/PhysRevD.105.084030 [arXiv:2105.00491 [gr-qc]].
- [21] H. Mouri and Y. Taniguchi, Astrophys. J. Lett. **566**, L17 (2002), [astro-ph/0201102 [astro-ph]].
- [22] A. L. Erickcek, M. Kamionkowski, and A. J. Benson, Mon. Not. Roy. Astron. Soc. **371**, 1992 (2006), [astro-ph/0604281 [astro-ph]].
- [23] N. Altamirano, D. Kubiznak, R. B. Mann, and Z. Sherkatghanad, Class. Quant. Grav. **31**,042001 (2014), [arXiv:1308.2672 [hep-th]].
- [24] S.-W. Wei and Y.-X. Liu, Phys. Rev. D **90**, 044057 (2014), [arXiv:1402.2837[hep-th]].
- [25] A. M. Frassino, D. Kubiznak, R. B. Mann and F. Simovic, J. High Energy Phys. **09**, 080 (2014), [arXiv:1406.7015 [hep-th]].
- [26] S. W. Wei, Y. Q. Wang, Y. X. Liu and R. B. Mann, Sci. China Phys. Mech. Astron. **64** (2021) no.7, 270411 [arXiv:2102.00799 [gr-qc]].
- [27] M. Tavakoli, J. Wu and R. B. Mann, JHEP **12**, 117 (2022) [arXiv:2207.03505 [hep-th]].
- [28] J. Wu and R. B. Mann, Class. Quant. Grav. **40** (2023) no.6, 06LT01 [arXiv:2208.00012 [gr-qc]].
- [29] J. Wu and R. B. Mann, [arXiv:2212.08087 [hep-th]].
- [30] C. Gao, Phys. Rev. D **104**, no.6, 064038 (2021)
- [31] R. Zwanzig, *Nonequilibrium Statistical Mechanics*, Oxford University Press (2001).